

The Lunar Mini-RF Radars: Hybrid Polarimetric Architecture and Initial Results

By R. KEITH RANEY, *Life Fellow IEEE*, PAUL D. SPUDIS, BEN BUSSEY, JASON CRUSAN,
J. ROBERT JENSEN, *Member IEEE*, W. MARINELLI, PRISCILLA MCKERRACHER,
CATHERINE NEISH, MARZBAN PALSETIA, RON SCHULZE, *Senior Member IEEE*,
H. BRIAN SEQUEIRA, *Member IEEE*, AND HELENE WINTERS

ABSTRACT | The two mini-radio-frequency (mini-RF) radars flown in near-polar lunar orbits (on Chandrayaan-1 and the Lunar Reconnaissance Orbiter) were the first of their kind, hybrid-polarimetric. This new paradigm transmits circular polarization, and receives coherently on orthogonal linear polarizations. The resulting data support calculation of the 2×2 covariance matrix of the backscattered field, from which follow the four Stokes parameters. These are the basis of science products from the observations, which include images that are traditional in radar astronomy, as well as polarimetric decompositions. The instruments all have mass less than 15 kg, antenna areas of about 1 m^2 , and modest power and spacecraft accommodation requirements. Data quality and instrument characteristics suggest that hybrid polarity is highly desirable for future exploratory radar missions in the Solar system.

KEYWORDS | Circular polarization ratio; polarimetric radar; radar astronomy; Stokes parameters; synthetic aperture radar

I. INTRODUCTION

The mini-radio-frequency (mini-RF) radar aboard India's lunar Chandrayaan-1 satellite [1] (2008–2009) was the first polarimetric synthetic aperture radar (SAR) outside Earth orbit. The architecture of that radar—and of its more advanced two-frequency sibling on the National Aeronautics and Space Administration (NASA) Lunar Reconnaissance Orbiter (LRO) [2] (2009–)—is hybrid dual-polarimetric [3], [4], a form of compact polarimetry [5]. The mini-RF systems, as the pioneers of this new class of radar, illustrate the value of hybrid polarity¹ for lunar and planetary applications.

Conventional dual-polarized remote sensing radars [6] transmit on one linear polarization (e.g., H) and receive on two polarizations: one matched to the transmitted polarization (H), and the other its orthogonal counterpart (V). Standard practice for large radar astronomical telescopes [7]–[9] is to use circular polarization on both transmit and receive. In contrast to both of these precedents, hybrid dual-polarimetric architecture receives orthogonal linear polarizations, while transmitting circular polarization.

An orbital radar that is expected to make radar astronomy-class measurements of the lunar surface should transmit circular polarization. However, the polarization

Manuscript received February 24, 2010; revised July 31, 2010; accepted September 16, 2010.

R. K. Raney, B. Bussey, J. R. Jensen, P. McKerracher, C. Neish, R. Schulze,

H. B. Sequeira, and H. Winters are with the Applied Physics Laboratory, Johns Hopkins University, Laurel, MD 20723-6099 USA (e-mail: k.raney@ieee.org; Ben.Bussey@jhuapl.edu; Bob.Jensen@jhuapl.edu; Priscilla.McKerracher@jhuapl.edu; Catherine.Neish@jhuapl.edu; ron.schulze@jhuapl.edu; Hermann.Sequeira@jhuapl.edu; Helene.Winters@jhuapl.edu).

P. D. Spudis is with the Lunar and Planetary Institute, Houston, TX 77058 USA (e-mail: spudis@lpi.usra.edu).

J. Crusan and **W. Marinelli** are with the NASA Headquarters, Washington, DC 20546 USA (e-mail: jason.crusan@nasa.gov; william.d.marinelli@nasa.gov).

M. Palsetia was with the Vexcel Corporation, Boulder, Co 80301-5730 USA. He is now with Microsoft Corporation, Redmond, WA 98052 USA (e-mail: marzpal@microsoft.com).

Digital Object Identifier: 10.1109/JPROC.2010.2084970

¹U.S. Patent 7 746 267, July 2010.

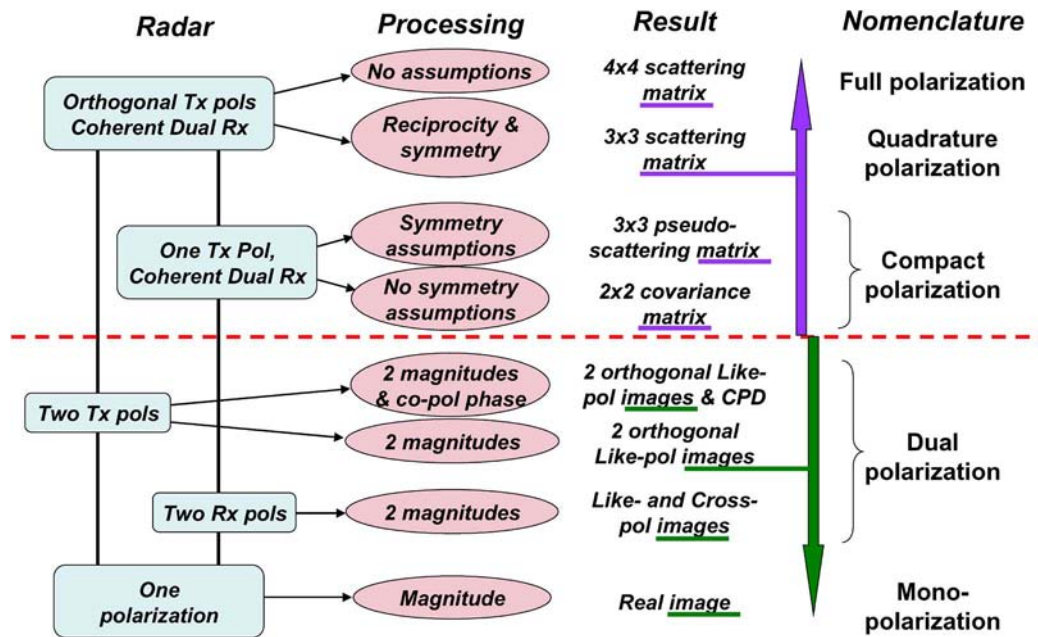


Fig. 1. The family of polarization diversity and polarimetric imaging radars.

basis of the receiver does not have to be circular, if the data product of the radar is stipulated to be the 2×2 covariance matrix of the backscattered field. This is true, because the values of the Stokes parameters obtained from the elements of the covariance matrix are independent of the particular polarization basis in which the data are observed [7], [10], [11]. The science products from the mini-RF radars are derived exclusively from information contained in the Stokes parameters. From this vantage point, the polarization plan of the mini-RF receivers was optimized with respect to engineering principles, without affecting science. Given that the transmitted polarization was to be circular, the optimum choice for the receiver was found to be orthogonal linear polarizations. The resulting hybrid polarimetric architecture has several advantages over alternatives, including self-calibration,² and simpler flight hardware.

The hybrid-polarimetric mini-RF radars offer the same suite of polarimetric information from lunar orbit as Earth-based radar astronomy, as justified in Appendix I. In particular, classical child parameters—such as the degree of depolarization, the degree of linear polarization, and the circular polarization ratio—may be determined from the Stokes parameters. The values of these parameters provide objective indications of geophysical properties of the surface [12]–[14].

This paper provides an introduction from a technical point of view to the mini-RF radars. Section II sets the stage with an overview of the family of polarimetric radars. Compact polarimetry is a subset of this family, of which

hybrid-polarity architecture is the relevant form. Section III summarizes the logical evolution from conventional radars to this new paradigm. Section IV describes the implementation of the mini-RF radar aboard LRO. Polarimetric data are useful only if they are relatively calibrated in phase and magnitude. Mini-RF calibration methodology and measurements are reviewed in Section V. Section VI offers examples of imagery and polarimetric interpretations of lunar data, followed by concluding remarks in Section VII. There are three appendixes that probe more deeply into particular specific topics: a polarimetric basis equivalence principle, the first-order impact of orbital velocity on a lunar or planetary SAR, and Stokes parameter formalism. An extensive list of references is included.

II. POLARIMETRIC IMAGING RADARS

In order to place the mini-RF radars in context, it is helpful to review the family of polarimetric imaging radars. Fig. 1 is a representation of all combinations of SAR polarizations from the standpoints of their diversity and data products. The simplest form of imaging radar transmits on one polarization, and receives on the same (like) polarization, for which there are many examples, such as Magellan [15], [16], RADARSAT-1 [17], or Seasat [18]. Conventional dual-polarized radars transmit on one polarization, and then receive simultaneously on two polarizations, one being the same as that which was transmitted, and the other its orthogonal counterpart, known respectively as the like- and cross-polarized channels. All prior Earth-oriented radar remote sensing systems have used linear polarizations, H

²See Section V.

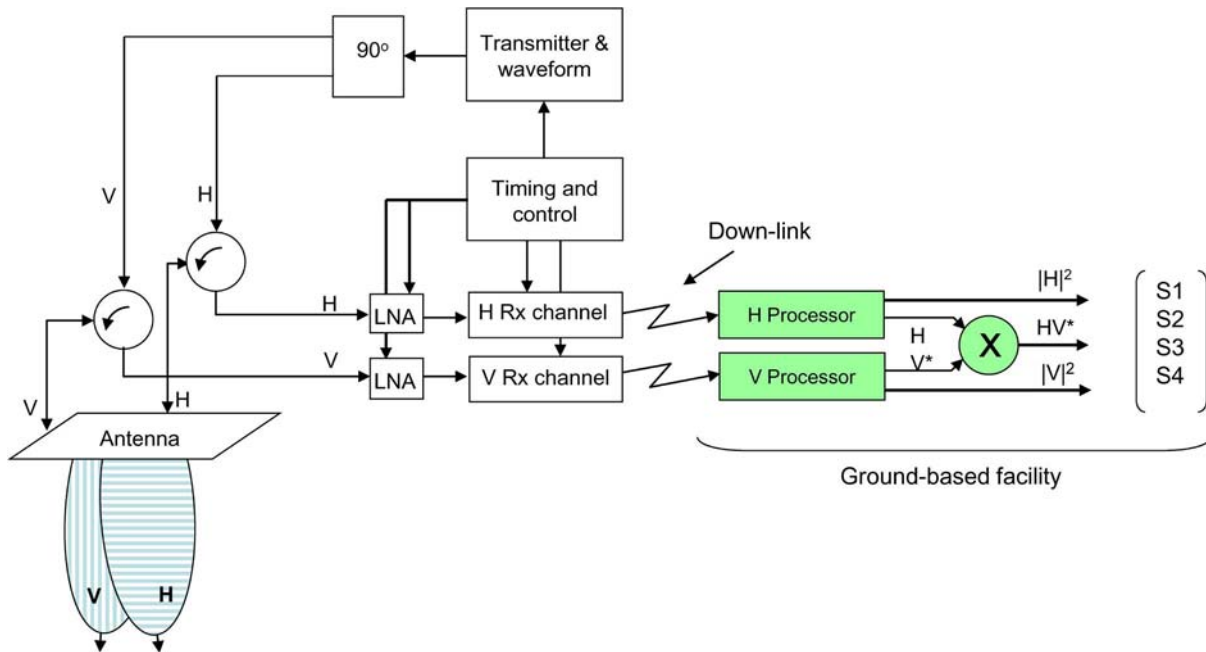


Fig. 2. Generic hybrid-polarimetric radar architecture.

and/or V. Typical dual-polarized examples include the airborne real aperture Ka-band APQ-97 flown by Westinghouse in the 1960s [19] and the alternating-polarization mode of Envisat ASAR [20]. Those two examples, although separated by nearly half a century, produce the same class of output, namely, like- and cross-polarized 2-D mappings of radar brightness. The figure includes variations on the theme of dual polarization, including transmissions that alternate between orthogonal polarizations. In all such cases, the data products can be described generically as “images,” since they do not include the relative phase between the two received channels. Consequently, analysis options are restricted essentially to ratios or differences of their respective images.

If relative phase is retained between the two received (orthogonal) polarizations, then a more appropriate descriptive terminology would be “polarimetric” since the data support certain quantitative measurements that are beyond the limited capabilities of simpler polarization-diverse imaging radars. In particular, the resulting data are sufficient to calculate the covariance matrix that corresponds to the polarimetric degrees of freedom of each type of SAR. In contrast to elemental imagery, such matrices are an entirely different class of data product. All radars above the dotted line in Fig. 1 are polarimetric.

The gold standard among polarimetric radars is the fully polarized case, at the top of the hierarchy shown in the figure. The intrinsic data product from this class of SAR is the 4×4 scattering matrix of each resolved element in the scene. After applying certain symmetry relations, this may be reduced to a 3×3 array, such as a

compressed Stokes matrix [21] or the compressed (Sinclair) scattering matrix [22]. These reduced forms are known commonly as quadrature-polarimetric SAR (quad-pol for short). In both the 4×4 and 3×3 data format cases the radar is the same; their difference resides only in the way their respective data products are prepared. Quad-pol SARs have attracted considerable attention since their introduction in the mid-1980s [23].

Compact polarimetry encompasses those options that fall between dual-polarized and quad-pol SARs. Compact polarimetric radars transmit on only one polarization, and receive on two orthogonal polarizations, retaining their relative phase. In the radar remote sensing world assumed (until about 2002) to include only linearly polarized systems, coherent dual-polarimetric imaging radar was disregarded.³ However, if alternative transmit polarizations (such as circular or 45° linear) are considered, then compact polarimetric radars deserve recognition as a potentially important SAR option [5]. The major motivation for compact polarimetry is to strive for quantitative backscatter classifications of the same finesse as those from a fully polarized system, while avoiding the principal disadvantages (mass, power, and limited coverage) associated with a quad-pol SAR.

III. EVOLUTION TO HYBRID POLARITY

It was known at the outset of the mini-RF project that those lunar radars had to be polarimetric, although their

³Numerous experiments showed that the relative phase between H- and V-polarized returns in response to transmission of either H or V polarization was random, hence conveyed little useful information.

TABLE 1 Mini-RF Top-Level Specifications

	Chan-1	LRO
Radar mass (kg)	9	14
DC power (W)	< 100	150
RF power (avg W)	15	25
Orbit altitude (km)	100	50
Tx/Rx polarization	Circular / H and V	
Antenna area (m ²)	1.1	1.1
Resolution (m) Baseline Zoom	150	150 15x30 (Az x Rng)
Looks (Baseline; Zoom)	16	16; 8
Swath (km)	~10	~10 (S Baseline) ~6 (C Baseline, & Zooms)
Sensitivity (NEqS ₀ , dB)	<-35	-30 & -25; -25 & -18
Wavelengths (cm)	12.6	12.6 & 4.2
Frequency (GHz)	2.38	2.38 & 7.14

particular form was undetermined. The early design studies looked carefully at alternative architectures, within the stipulated science and implementation constraints. The implementation requirements included minimal mass and power, and accommodation for the dual-linearly-polarized (H and V) antenna design that had been stipulated as part of the technology demonstration that was a parallel theme of the mission. The first-order science requirement was measurement of the circular-polarization ratio (CPR), defined as the power ratio of the same sense (SC) to the opposite sense (OC) of circularly polarized backscatter, relative to the sense of the transmitted circular polarization. This measurement requires transmission of circular polarization.

The original concept for the mini-RF radars [24] was patterned after conventional Earth-based radar astronomical instruments, which transmit right-circular polarization (or left-circular polarization), and receive both senses of circular polarization, resulting in SC and OC image pairs. Circularly polarized transmission may be realized by transmitting H and V polarizations simultaneously, 90° out of phase. These signals are generated by running the output of the transmitter through a 90° hybrid. If the radar were required to be circularly polarized on receive as well as on transmission, then the H and V signal sequences from the antenna both would have to go through another 90° hybrid, from which the outputs would be combined to generate signals at both senses of circular polarization, resulting in a circularly polarized dual-channel receiver.

The mini-RF architecture introduced a paradigm shift in the design of imaging radars. Their primary data product was stipulated to be the 2 × 2 covariance matrix of the backscattered field. Given that condition, the polarization

basis of the receiver becomes irrelevant, because the four-element Stokes vector calculated from the covariance matrix does not depend on the polarization basis in which the data are observed [7]. It follows that the polarization basis of the mini-RF receivers could be chosen to optimize the hardware.

By keeping the H- and V-polarized data received at the antenna in their linear polarizations all the way through the receiver and the processor, the conventional circularly polarized approach was simplified. In particular, staying linearly polarized on receive meant that the two 90° hybrids could be eliminated in the receive paths [4]. This simplification not only reduced the mass of the radar, but also improved the receiver's noise figure. Since the Stokes vector captures all of the information available in the backscattered field, the resulting data products offer more measurement options⁴ than the usual SC and OC image pairs. The mini-RF hybrid-polarity architecture is an ideal response to the top-level requirements—maximal science provided through minimal hardware.

IV. IMPLEMENTATION

Although the two mini-RF radars share the same polarimetric architecture, their performance and implementation differ in specifics (Table 1). The version that flew on India's Chandrayaan-1 spacecraft only had one spatial resolution (150 m) and one frequency (S-band), consistent with Magellan's precedent [16]. This instrument is known by two names, either mini-SAR (ISRO⁵) or Forerunner

⁴See Appendix III.

⁵Indian Space Research Organization

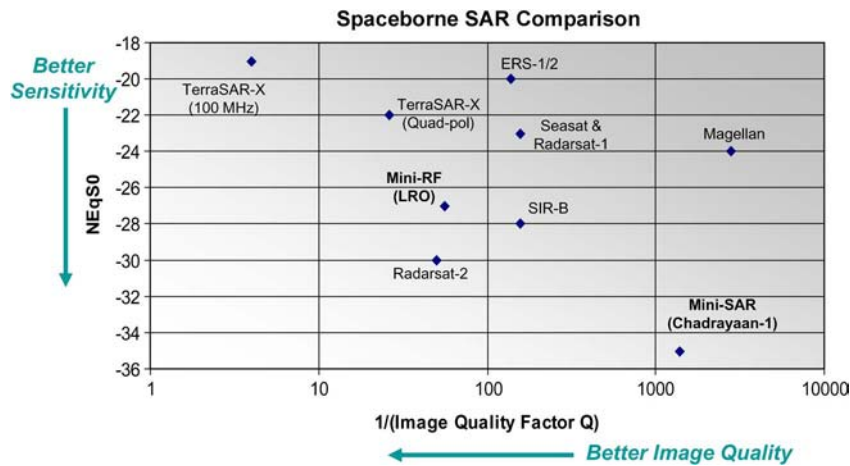


Fig. 3. SAR comparison chart.

(NASA). In contrast, the system on NASA’s LRO was a technology demonstration, reflected in its formal name mini-RF.⁶ That system had two resolutions (baseline and zoom), two frequencies,⁷ and extra functionality. The second frequency on LRO was chosen to be as close to X-band as possible, while still fitting within the controlling bandwidth of the transmitter, which led to a threefold frequency spread. Two frequencies precipitated different approaches between mini-RF and Forerunner for their respective antennas and transmitters. The bandwidth in LRO’s zoom mode (10 MHz) was limited above by frequency allocation protocols, which, surprisingly, are applicable in the lunar environment. Both systems had nominal design lifetimes of three years.

The mini-RF radars used burst mode [25] in which temporally separated groups of pulses are transmitted. In this mode, burst length determines the azimuth resolution of the image data, and burst period determines the number of looks. In addition, the LRO radar included a mode in which a uniform pulse-repetition frequency (PRF) was maintained for an entire pass, thus providing data suitable for interferometric SAR analysis [26]–[28]. Both builds included waveforms that would accommodate nadir-viewing data collects. Finally, the LRO mini-RF was motivated in part by a requirement to demonstrate that one instrument could fill two roles, serving either as an imaging radar or as a communications subsystem.

It is instructive to compare the performance of these lunar radars with other orbital SARs. Two fundamental quantitative indices of an imaging radar’s “goodness” are *sensitivity* and *image quality*. Sensitivity is measured by noise-equivalent sigma-zero (NES0), which is the level of

the weakest radar backscatter whose value is equal to the additive noise within the radar [29]. Smaller NES0 is better. From the information content point of view,⁸ image quality (Q_{SAR}) is quantitatively measured by the number of statistically independent looks, divided by the product of range and azimuth resolution [6], [30]. Larger Q_{SAR} is better. In Fig. 3, these norms are used to compare the performances of the mini-RF and the mini-SAR with several well-known SARs [30], including Magellan [15], which is the best example of a planetary radar imager.

What justifies the mini moniker for these radars? They are indeed small by space-borne radar standards, having mass less than 15 kg each.⁹ There are two factors. The primary reason that these radars can be “mini” is that any spacecraft in lunar orbit has relatively small velocity and low altitude. (Appendix II reviews the governing expression for spacecraft on-orbit velocity, and offers a tabular comparison for several bodies in the solar system, including the Earth and the Moon.) A SAR’s minimum antenna area is proportional to the radar’s velocity-altitude product [29]. At the Moon the minimum antenna area for a SAR antenna (at S-band) is much less than 1 m², in contrast to a similar radar in Earth orbit for which the minimum area must be larger by a factor of 35.

The secondary reason that the lunar radars have low mass is that their design and hardware were required to comply with strict mass allocations. However, none of the components are built of “unobtainium,” and none incorporate particularly advanced technology.

⁸Image quality also depends on engineering factors, including relative sidelobe and ambiguity levels. However, parameters such as those are acceptable for all radars of interest, and so are disregarded here since they do not contribute to quantification of the applications-oriented information content of the data products.

⁹For comparison, the mass of Radarsat-2’s antenna alone is 784 kg, having an area of about 15 m², but it is an active phased array, which also increases its mass relative to that of any simpler structure.

⁶In this paper, the term mini-RF may be either specific to the LRO instrument, or generic, encompassing both builds, depending on context.

⁷The second frequency for historical reasons often is stated as X-band (~3-cm wavelength), whereas as built it is actually C-band (~4-cm wavelength).

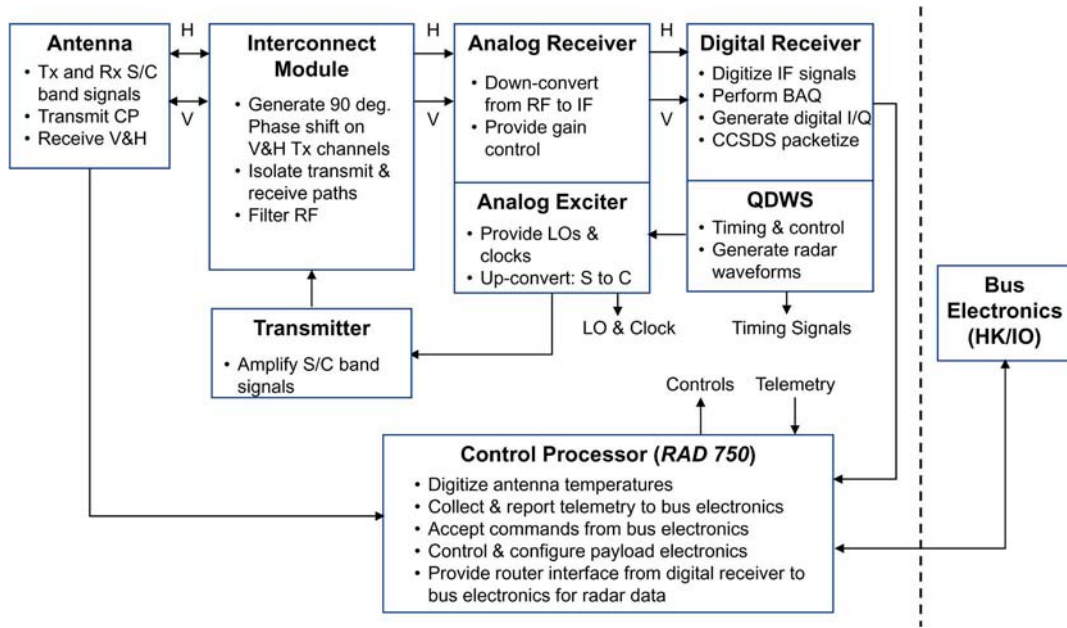


Fig. 4. Mini-RF functional radar block diagram.

As illustrated in its functional block diagram (Fig. 4), the LRO mini-RF radar comprises eight subsystems, interfaced with the spacecraft through the bus electronics assembly. The prime contractor developed the specific requirements and interfaces for all subsystems, which were provided to the project from a variety of specialized vendors. Fig. 5 shows the LRO spacecraft during its integration, assembly, and test phase. The radar’s antenna

(wrapped in its thermal blanket) is a prominent feature of the flight assembly. The radar is packaged in three separate units, mounted on an isothermal structural panel (out of sight behind the folded solar array). The antenna’s long dimension of 1.6 m, together with the technicians standing nearby, provide an indication of scale.

The antenna design was based on an “egg crate” format (Fig. 6), chosen to support broadband (dual frequency) performance with a single antenna panel, while also meeting stringent mass and form-factor constraints. (Given the available space for the radar aboard LRO, alternative approaches, such as center- or offset-fed reflectors, would have required on-orbit deployment, a complication to be avoided if possible.) The mini-RF antenna as built had low mass (4 kg), and acceptable gain, efficiency, and polarimetric radiation patterns.



Fig. 5. LRO during final integration, assembly, and test.

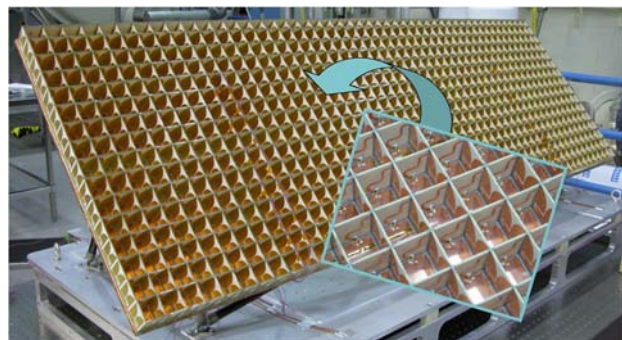


Fig. 6. The mini-RF “egg crate” antenna.

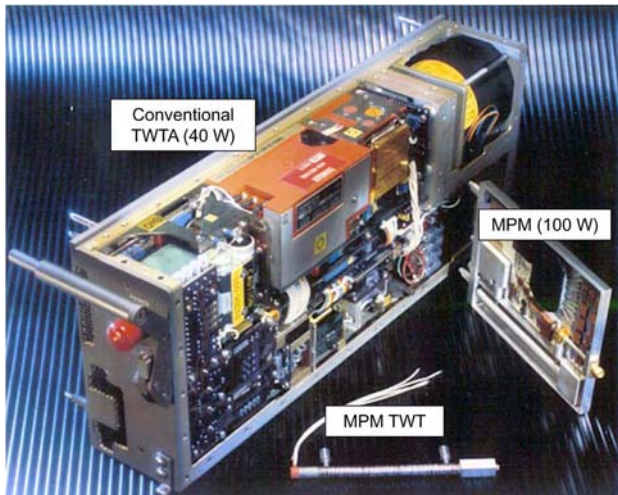


Fig. 7. Comparison of TWTA and MPM technologies.

The LRO mini-RF transmitter design used microwave power module (MPM) technology [31], [32]. This approach was ideal for the lunar application, since it provided the required power with compact form, low mass, and efficient hardware, and had sufficiently wide bandwidth to accommodate both LRO frequencies. The MPM (Fig. 7) combines a solid state RF driver/preamplifier with a traveling wave tube (TWT), taking advantage of the best features of both solid state and vacuum electronic technology. A conventional TWT amplifier (TWTA) approach would have been larger and more massive, neither of which could have met requirements. MPM technology has extensive heritage in airborne systems, but the mini-RF development program included tasks to adapt the basic design for spaceflight. Primary challenges to be overcome were use of space-qualified materials and components, qualification for operation in deep vacuum, and reliability. The lunar radiation environment presented a particular challenge; parts were screened to tolerate a total dose of 20 krad, to suffer no destructive latch up, and to be tolerant of nondestructive latch up to 75 MeV. The MPM thermal design necessitated integration with the heat pipe system that was part of the isothermal mounting panel on the LRO spacecraft.

Although a few parts required waivers, the vast majority were accepted to standard Class S requirements, with de-rating criteria in accordance with established procedures. Mini-RF uses plastic encapsulated microcircuits (PEMs) with the screening operable over the temperature range from $-55\text{ }^{\circ}\text{C}$ to $+125\text{ }^{\circ}\text{C}$ (ambient atmospheric pressure).

The digital receiver and quadrature digital waveform synthesizer (QDWS), based on airborne radar heritage, were adapted to lunar orbital requirements. These systems enabled the flexibility and reprogrammability required by the mini-RF system in LRO's low-altitude lunar orbit. That

environment is especially challenging for radar design, because the orbit altitude may vary $\pm 20\%$ relative to its nominal 50 km above the mean lunar radius, the Moon's topographic relief is on the order of 10 km, and the radar (at its nominal 45° -incidence) has relatively narrow swaths (usually less than 10 km, according to mode). Nearly 1000 preprogrammed waveform combinations (primarily PRF, range gate setting, and burst parameters) were required to ensure that: 1) the timing in slant range was correctly set to collect data from the lunar surface; 2) the reflection from nadir did not arrive at the same time as the intended data; 3) the receive window occurred in an interval between transmitted pulses; 4) the PRF was neither too high (which would generate range ambiguities) nor too low (which would generate Doppler ambiguities); 5) the burst length and period would support the resolution and number of looks desired in the final image products; 6) the radar would operate correctly at the higher orbits expected during commissioning and the extended mission; and 7) data could be collected when nadir-viewing. Waveforms were preselected based on orbit ephemeris and lunar topographic relief, and uploaded to the radar, one waveform per each 4-min (nominal) imaging pass.

To limit the data volume per collection session, the digital receiver had the added task of data compression prior to storage and telemetry. The only feasible near-lossless method to compress raw SAR signals is to reduce the number of digital bits per (complex) sample. Mini-RF used a form of block-adaptive quantizer (BAQ), in principle similar to that pioneered by Magellan [33], to reduce the inherent 8-b quantization to as few as 2 b, according to imaging mode. More bits, as would be preferable for an interferometric data take, could lead to a corresponding reduction in swath length, if constrained by on-board data storage capacity.¹⁰

V. RELATIVE CALIBRATION

Polarimetric measurements imply more stringent calibration of the radar than required by a single channel system, since quantitative polarimetric measurements depend on the relative phase and magnitude between signals in the two receive channels. Hybrid-polarimetric architecture has the unique and appealing property that it is self-calibrating, at least in principle¹¹ [4].

Calibration of the mini-RF instruments proved challenging for several reasons. Prior to launch no opportunities for end-to-end measurements of the complete radar system were available; only standalone characterizations of the radar electronics and antenna were possible. Once in flight, conventional calibration techniques used by Earth

¹⁰In practice, data volume constraints for the LRO mini-RF have been more generous than indicated during preflight mission planning.

¹¹A complete calibration using only nadir measurements would be possible if and only if the radar were hybrid-polarimetric, and known to transmit high-fidelity circular polarization.

orbiters [34] were not an option for the mini-RF radars, as there are no Amazon rain forests or calibrated radar reflectors available on the Moon. Therefore, the team employed a unique combination of experiments, designed specifically to measure the key relative calibration parameters. The mini-RF calibration campaign included direct and separate characterizations of the transmit and receive portions of the radars via Earth-based resources, hence obviating the assumption of perfect circularity of the transmitted signal from the calibration analysis. The two mini-RF radars are the pioneers of this calibration strategy.

The on-orbit calibration experiments measured the mini-RF receive and transmit characteristics on separate days, using different Earth-based antennas, as the corresponding transmitter or receiver platforms. The Arecibo Radio Telescope (ART) in Puerto Rico acted as a transmitter to the mini-RF receiver. The Green Bank (Radio) Telescope (GBT) in West Virginia received mini-RF transmissions. For both sessions, the spacecraft was maneuvered to generate cross sections of the elevation and azimuth antenna patterns. Effects due to the Earth’s ionosphere proved to be negligible. Fig. 8 shows typical results for the mini-RF radar on LRO.

In a separate operation, the spacecraft was rolled to point the radar antenna towards the Moon at nadir. In this orientation, the expected radar backscattering properties in the H and V polarizations are known to be (on average) the reflection of the transmitted signal, comprising a practical means of collecting an end-to-end data set of known characteristics. In the hybrid-polarity architecture, these signals should have the opposite circularity relative to the

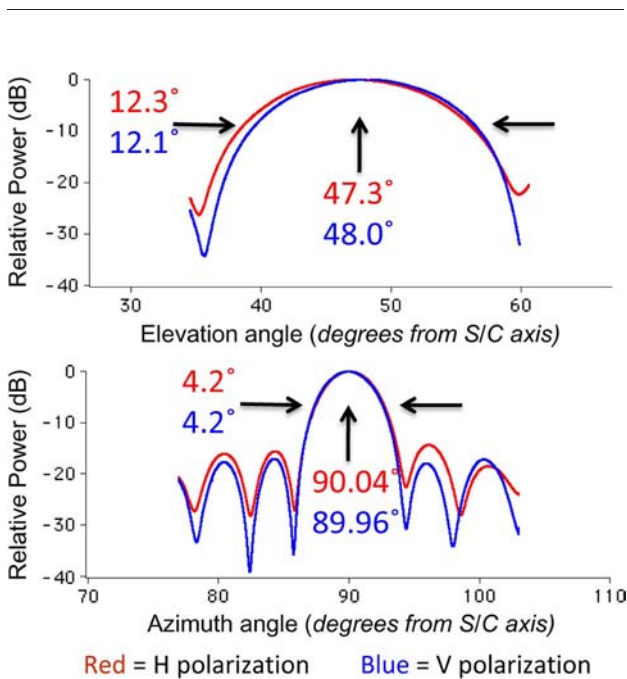


Fig. 8. Mini-RF antenna patterns observed through illumination from Arecibo.

TABLE 2 Top-Level Calibration Observations Measured for Mini-SAR on Chandrayaan-1

(a)		
Rx Chain Parameter	Nominal Value	
V/H imbalance	0.3	0.2 dB
V-H phase imbalance	43.5°	1.5°

(b)		
Tx Chain Parameter	Nominal Value	
V/H imbalance	-2.44	0.2 dB
V-H phase balance	-92.4°	0.5°
Axial Ratio	2.46	0.15 dB

(c)		
Parameter	End-to-end prediction	Nadir Observation
V/H gain balance	-2.14 0.25 dB	-2.55 0.25 dB
V-H phase balance	-135.9° 1.5°	-138° 2.7°

transmitted field, and should be statistically identical to first and second order [4]. Measurements from the nadir data collection allowed comparisons of those data with the calibration responses derived through ART and GBT.

The data in Table 2 verify that the top-level results for phase and amplitude balance derived through the nadir-viewing method and the external illumination method compare very well. In addition, prelaunch measurements of phase and amplitude balances for the transmitter, receiver, and antenna chains provided a prediction on the sensitivity of these items to temperature and other second-order variations. For the LRO mini-RF, a built-in loop-back calibration mode provided a means to compare on-orbit performance of the electronics with prelaunch measurements.

Once their values are determined, phase and amplitude imbalances for the complete receive sequences (antenna to end output) can be fully compensated in the processor by application of correction coefficients. Fig. 9 shows the results of phase correction observed in data from mini-SAR. The radar transmits (nominal) left-circular polarization, which would have a V–H relative phase of +90°. The sense of polarization is reversed upon reflection, so, on average, the mean phase observed in the received data should be of OC, having a sign of −90°, which the data bear out.

Imperfect phase and amplitude characteristics in the receive chain, once known, can be removed through application of the appropriate calibration compensations. However, if the transmitted polarization does not have perfect circularity (unity axial ratio, or 0 dB), then polarimetric analysis may be compromised. The calibration data showed that the circularity of the transmitted polarization was less than perfect, having an axial ratio on

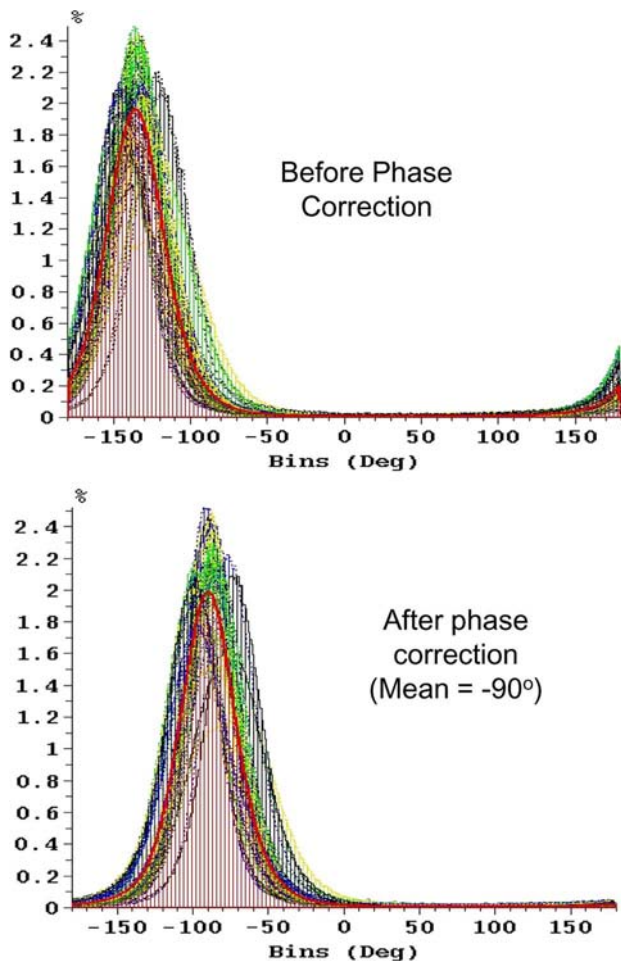


Fig. 9. Phase distributions observed for mini-SAR before and after first-order phase calibration.

the order of 2.5 dB for both radars. Analysis shows that this level of axial ratio has relatively little effect for certain measurements. For example, the data in Fig. 10 illustrate that the CPR is affected far less by the transmitted axial ratio than by the polarimetric properties of the lunar surface, for which 0.6 is the average value of the degree of polarization m [see (7) in Appendix III]. This relatively low value of m is attributed to the regolith¹² that gives rise to volumetric radar backscatter, thus randomizing the observed polarization properties of a portion of the reflections.

VI. RESULTS

Stokes parameters (Appendix III) capture all of the information embedded in the backscattered field, and are the foundation for all data products from the mini-RF radars. The Stokes parameters may be calculated from the

¹²Regolith is the standard terminology (since about 1895) for the layer of loose dust and heterogeneous materials covering the more solid rock below.

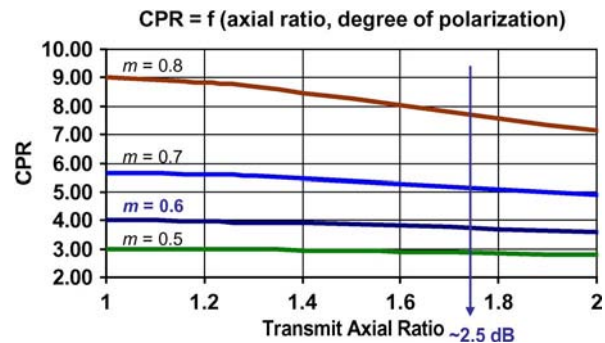


Fig. 10. Circular polarization ratio as a function of degree of polarization m and transmitted axial ratio. (The actual values of CPR depend also on the dielectric properties of the materials.)

data available at the output of the ground-based mini-RF processor (Fig. 2), according to

$$\begin{aligned}
 S_1 &= \langle |E_H|^2 + |E_V|^2 \rangle \\
 S_2 &= \langle |E_H|^2 - |E_V|^2 \rangle \\
 S_3 &= 2\text{Re}\langle E_H E_V^* \rangle \\
 S_4 &= -2\text{Im}\langle E_H E_V^* \rangle
 \end{aligned} \tag{1}$$

where the $\langle \rangle$ indicate averages, which are essential to reduce the standard deviation of the parameter values. Each of these parameters is an elementary combination of two numbers, drawn from the powers (real) in the two channels, and the cross product of their (complex) amplitudes. The cross product (or equivalently, the corresponding differential phase) consists of two real numbers, the signed amplitudes of its real and imaginary components. The resulting set of four real numbers, evaluated at each pixel location in the multilook image domain (and spatially averaged as appropriate), support specific representations (Appendix III) of the observed data, including total backscattered power (S_1), circular polarization ratio (CPR), OC and SC imagery, and the like.

The conventional data product from Earth-based radar astronomy is a reflected power mapping of the backscattered field observed in the OC of circular polarization relative to that which was transmitted. The same product can be derived from the mini-RF radars, in spite of their linearly polarized receivers. The OC image (given that the transmission is left-circularly polarized) is given by S_1 – S_4 (Appendix III). An example is shown in Fig. 11, the Bessel crater,¹³ compared to an optical image of the same feature [35]. In this image, the radar is viewing the scene from the left, so the near wall of the crater is shadowed, while the far wall (just outside the frame) is more brightly illuminated. Since the radar’s incidence is known, the steepness

¹³Depth 1.7 km, diameter 16 km, coordinates 21.8° N, 17.9° E.

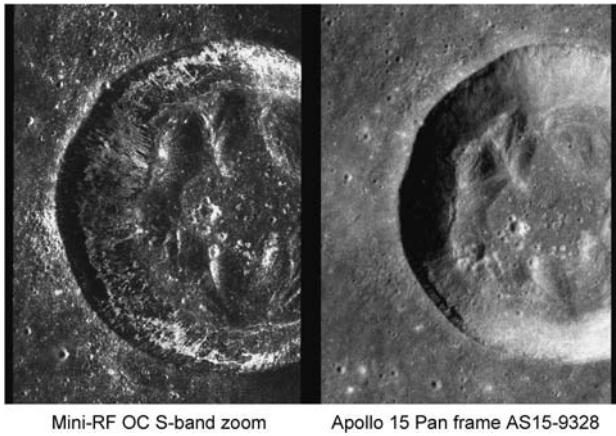


Fig. 11. Bessel crater, portrayed in opposite-sense (OC) polarization.

of the near wall may be estimated from the shadow. The “radar-bright” features in the floor of the crater correspond to features seen in the optical frame.

S-band zoom is the favored mode for the LRO mini-RF radar, due to its frequency compatibility with Chandrayaan-1’s data, but also due to its outstanding data quality. One mission objective was to assemble mosaics of both polar regions at the same frequency, resolution, and nominal incidence. Hence, once data collections begin in one mode, then that mode dominates subsequent data collections for an entire polar imaging season. Imaging seasons have duration of about one month, and are separated by six months, due to constraints levied by the relative orbit plane-to-sun angle.

One of the objectives of the mini-RF radars was to highlight areas of high CPR. This parameter may be calculated from the Stokes parameters (Appendix III), and portrayed visually in a polarimetric interpretation. Fig. 12 shows a mosaic of LRO mini-RF S-band zoom data for regions near the lunar south pole. The calibrated data are color coded to indicate the estimated values of CPR. The data were collected as strips on consecutive orbits, then assembled. These strips appear to be radially distributed, which is a consequence of the slow rotation of the Moon (1° per orbit cycle) beneath the satellite in its near-polar orbit plane. The nonimaged area centered on the pole is a result of the viewing geometry of the radar, which, being side-looking, cannot image the pole itself. The nonimaged area is irregular in shape, because the orbit’s inclination is perturbed (over a 14-day period) by the Moon’s gravity field. Such near-pole regions can be partially imaged by spacecraft maneuvers to enable steeper incidence viewing, especially when the orbit’s inclination and spacecraft orientation would favor data collection closer to the pole.

Interpretation of the data to highlight elevated CPR is more effective in larger scale imagery. Fig. 13 shows a

group of passes through Peary,¹⁴ which is the largest impact crater close to the north pole [35]. The floor of Peary hosts many small impact craters whose diameters are as small as 1 km, and whose interiors are deemed to be permanently shadowed. Pixels having high CPR appear as red in this calibrated polarimetric interpretation. The data may be parsed to show the distribution of CPR values corresponding to their locations, either inside or outside the craters. High CPR values are more dominant in the interiors. Hence those high CPR values are of particular interest, because they are consistent with the signature expected from volumetric deposits of water–ice [8], [36].

The Stokes parameters support several less conventional analysis alternatives, a key one of which is the degree of polarization m [see (7) in Appendix III]. This parameter is larger for backscatter from hard surfaces, and smaller for backscatter from complex random surfaces, especially those populated by lunar regolith. Fig. 14 is an example of a degree-of-polarization product selected from mini-SAR data (S-band) of the north pole.

VII. CONCLUDING COMMENTS

The mini-RF radars on Chandrayaan-1 and the LRO have proven to be very successful, meeting or exceeding their design requirements and expectations. Their hybrid–polarity architecture is the first demonstration of this design paradigm from orbit. They afford the first polarimetric radar observations of the entire Moon, including especially the lunar poles and far side. The results are providing new information and opening new insights into the lunar surface.

From a technical point of view, the mini-RF radars have pioneered several innovations. They have been exercised in unique calibration modes that do not depend on the usual *in situ* references of an extended distributed backscattering feature (such as the Amazon rain forest) or a calibrated point reference (such as a corner reflector or active radar calibrator). For lunar or planetary polarimetric radars, calibration methodologies are required that do not require known references in the scene. By taking advantage of the polarization basis independence of the Stokes parameters of the received data, the mini-RF systems are more capable instruments than all previous radars that have ventured outside Earth orbit, yet their implementation is relatively simple, an attribute that is especially appealing for planetary deployments.

Although for both radars the observed transmitted field is elliptically polarized rather than purely circular, simple polarimetric analysis such as estimation of CPR seems relatively robust to this imperfection. Other Stokes-based measurements may be more sensitive to imperfect circularity of the illuminating field. Any future opportunity

¹⁴Diameter 73 km, coordinates 88.6° N, 33.0° E.

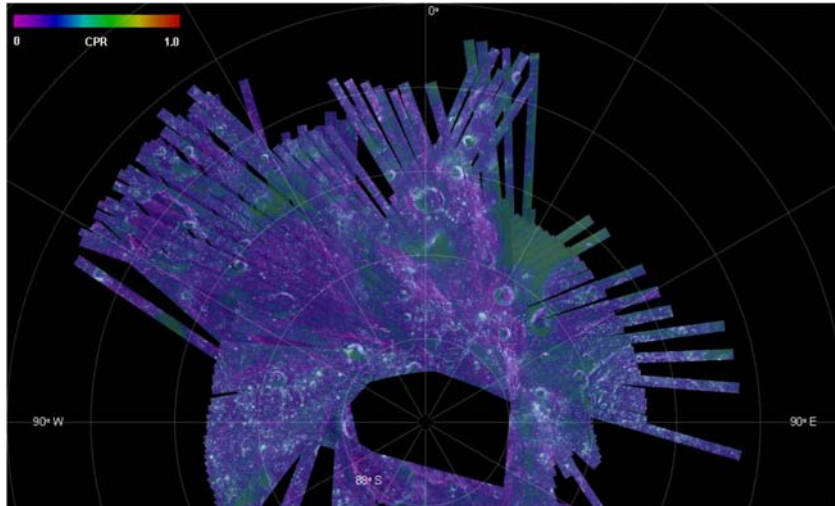


Fig. 12. Mosaic of LRO S-band data from the lunar south polar region (grid spacing 50 m/pixel, after averaging).

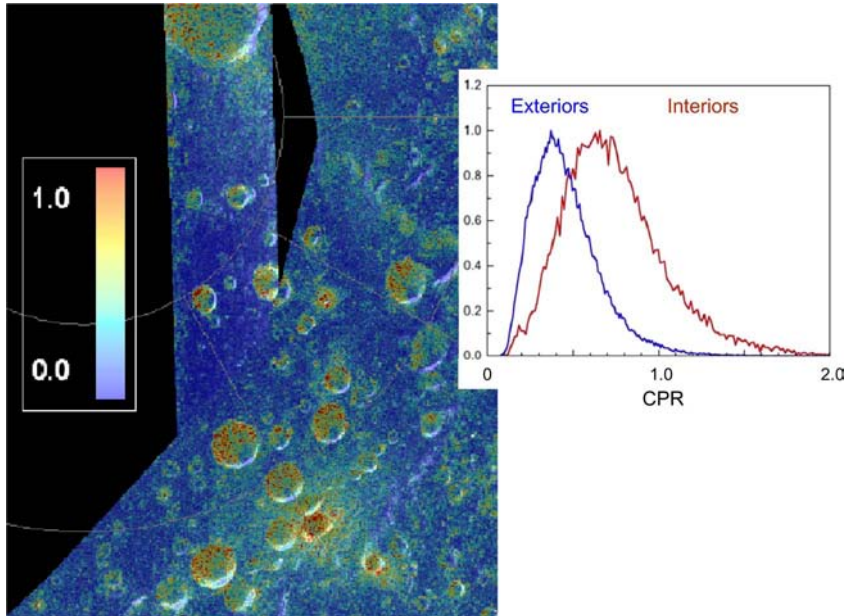


Fig. 13. Calibrated CPR interpretation of a portion of the floor of Peary, showing a statistically significant predominance of elevated CPR values from the interiors of smaller craters that are always shadowed from solar illumination.

for hybrid-polarimetric radar architecture should assure that the aspect ratio of the transmitted field is close to unity. ■

APPENDIX I POLARIZATION BASIS EQUIVALENCE

Consider the two forms of compact polarimetry that transmit circular polarization: one that receives orthogonal circular polarizations (CC), and the other that receives orthogonal linear polarizations (CL). The CC paradigm

characterizes traditional radar astronomy [8]. If a radar supports generation of the covariance matrix of the received data, then these two architectures generate data that have virtually identical information content.

At first glance it may seem bizarre to claim that very massive Earth-based radar astronomy facilities (such as the 300-m diameter Arecibo Radio Telescope in Puerto Rico) holds a fundamental one-to-one relationship to spaceborne radars such as mini-RF, yet it is so. The Arecibo facility can hardly claim to be a compact radar, yet it is by far the best established example of compact polarimetry.

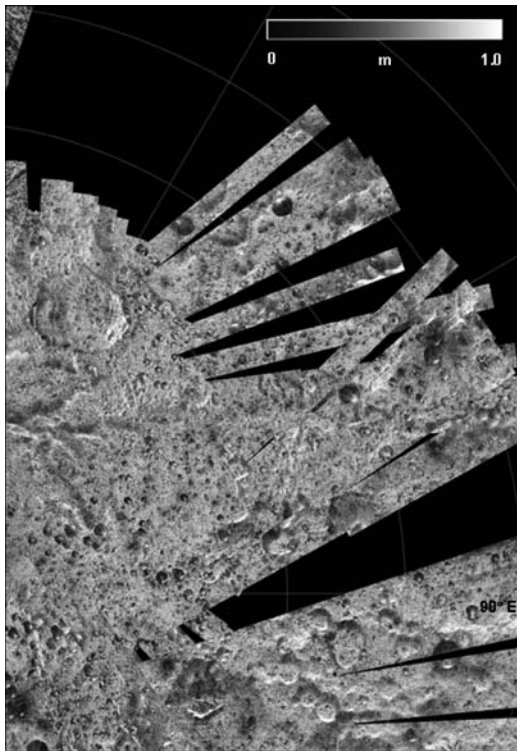


Fig. 14. Mini-SAR S-band data from near the north lunar pole, interpreted by degree of polarization m (grid spacing 75 m/pixel).

Well-established best practice in radar astronomy is based on analysis of the four-element Stokes vector that characterizes the radar backscatter observed from selected bodies, such as the Moon or Venus [37] in response to circularly polarized transmissions. The first Stokes component conveys the total backscattered power, thus similar in appearance to the data collected by a mono-polarized imaging radar, such as Magellan. The remaining three Stokes parameters express quantitatively how the radar's illumination of the scene is redistributed into the backscatter's polarimetric constituents.

Recall from classical physical optics that the values of the four Stokes parameters do not depend on the polarization basis in which the quasi-monochromatic electromagnetic (EM) field is observed [11]. This fact implies, given that the radar transmits circular polarization, that the same Stokes parameters can be evaluated from data collected by either a circularly or a linearly polarized coherent receiver. This conclusion justifies the claim that classical radar astronomy provides prime precedent for the dual-polarimetric hybrid-polarity architecture of the mini-RF radars.

It is straightforward to illustrate the point with an example. The data collected by any fully polarized SAR can be manipulated (by polarization synthesis [23]) to replicate the response to circularly polarized transmission by either a circularly polarized or linearly polarized receiver.

Hence, quadrature-polarimetric airborne SAR data¹⁵ may be used to create both CC and CL Stokes parameters of the same scene. Once evaluated, these may be compared directly, as in Fig. 15, in which the CC and CL values are mapped onto the horizontal and vertical axes, respectively. The ideal distribution of the resulting values for each Stokes parameter would fall on the diagonal line of equivalence. The measured distributions follow that prediction essentially perfectly, thus verifying that analysis of real data illustrates Stokes parameter invariance with respect to the observation basis.

APPENDIX II ALTITUDE-VELOCITY FACTOR

The performance of range-Doppler radars such as the SARs aboard the lunar spacecraft is conditional upon the velocity of their host platforms. The velocity of a spacecraft in orbit at altitude h above a planet of radius R_p and mass M_p is given by

$$V_{SC} = \sqrt{M_p G / (R_p + h)} \quad (2)$$

where G is the universal gravity constant: $6.67 \times 10^{-11} \text{ Nm}^2 \text{ kg}^{-2}$. Table 3 lists representative spacecraft velocities for bodies in the solar system that have been visited, or are likely to be observed, by remote sensing radars. Feasible satellite altitudes are limited below by the prevailing atmospheric density. The final column of the table lists the altitude-velocity product hV_{SC} corresponding to each entry. This product is a scaling factor that characterizes the range-Doppler environment within which the orbital radar must operate. There is approximately a 40-fold spread in the value of this parameter, from the Earth to Jupiter's moon Europa. It follows that radar designs that work in one situation may not be at all appropriate if migrated to a different planetary body.

The issue is well illustrated by the lower bound on the area of a SAR antenna. The constraint is given by [29]

$$\text{Area}_{\text{ANT}} > 4RV_{SC} \left(\frac{\lambda}{c} \right) \tan \theta_{\text{inc}} \quad (3)$$

where R is radar range, which for side-looking SAR geometry is always larger than the spacecraft's altitude h . Thus, the antenna area lower bound is proportional to the height-velocity factor. From the table, it may be seen that the difference in this factor between the Earth and the Moon is of order 35, which means that the antenna area of an orbital lunar SAR can be 35 times smaller than its counterpart in Earth orbit. This is the primary reason that

¹⁵In this example, data are used that were collected in October 2008 by a quad-pol airborne L-band radar over Meteor Crater in Arizona.

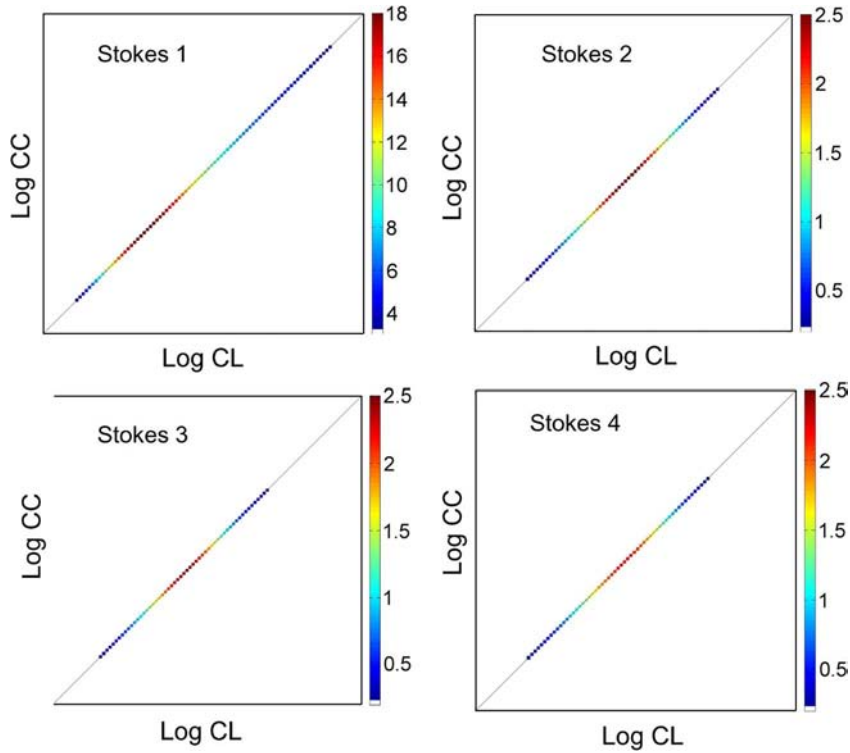


Fig. 15. The four Stokes parameters, evaluated from real radar data, show that values derived from a circularly polarized receiver are equivalent to those derived from a linearly polarized receiver, in response to circularly polarized transmissions. (Since the Stokes parameters 2, 3, and 4 may be either positive or negative, their comparisons are calculated using absolute values.)

the mini-RF radars are so small, at least relative to well-known SARs such as Radarsat-2 or Envisat.

APPENDIX III STOKES PARAMETER ANALYSIS

The theory represented by the Stokes parameters is well-known [38]. A monochromatic EM field is repre-

sented by the ellipse swept out by its electric potential vector $\mathbf{E} = [E_x \ E_y]^T$. In general analytic form, the orthogonal components of \mathbf{E} are

$$\begin{aligned} E_x &= a_1 \exp j(\tau + \delta_1) \\ E_y &= a_2 \exp j(\tau + \delta_2) \end{aligned} \quad (4)$$

TABLE 3 Orbital Radar Height-Velocity Factors

Body	Mass (kg)	Radius (km)	Altitude h (km)	V (m/s)	hV (km ² /s)
Earth	5.97E+24	6380	800	7466	6000
Venus	4.87E+24	6052	300	7151	2200
Mars	6.4E+23	3397	400	3353	1600
Titan	1.35E+23	2575	200	1801	360
Ganymede	1.4E+23	2631	100	1849	185
Calisto	1.08E+23	2400	100	1697	170
Moon	7.35E+22	1737	100	1634	160
Europa	4.8E+22	1569	100	1385	140
Enceladus	1.08E+20	504	100	109	11

where τ represents the EM oscillation, and $\delta_2 - \delta_1 = \delta$ represents the relative phase between the two components. Stokes [10] proved that such a field could be represented by four real numbers, known as the Stokes parameters (S_1, S_2, S_3, S_4). These often are represented as $\mathbf{S} = [S_1 \ S_2 \ S_3 \ S_4]^T$ which is a logical vector, where T denotes transpose. In this formalism, the Stokes parameters (expressed in the BSA convention appropriate for radar backscatter geometry [7], [39]) are

$$\begin{aligned} S_1 &= \langle a_1^2 \rangle + \langle a_2^2 \rangle = J_{xx} + J_{yy} \\ S_2 &= \langle a_1^2 \rangle - \langle a_2^2 \rangle = J_{xx} - J_{yy} \\ S_3 &= 2\langle a_1 a_2 \cos \delta \rangle = 2\text{Re}J_{xy} \\ S_4 &= -2\langle a_1 a_2 \sin \delta \rangle = -2\text{Im}J_{xy} \end{aligned} \quad (5)$$

where the $\langle \dots \rangle$ indicate temporal (or locally spatial) averages, and the several J terms indicate elements of the Hermitian covariance matrix $\mathbf{J} = \langle \mathbf{E} \cdot \mathbf{E}^{*T} \rangle$ [11], [40].

We posit that the SAR's transmitted field is left-circularly polarized (L), as is the case for the mini-RF radars. Starting from focused, single-look complex data, the four Stokes parameters, in either the linear or the circular polarization bases at the receiver, are

$$\begin{aligned} S_1 &= \langle |E_H|^2 + |E_V|^2 \rangle = \langle |E_L|^2 + |E_R|^2 \rangle \\ S_2 &= \langle |E_H|^2 - |E_V|^2 \rangle = 2\text{Re}\langle E_L E_R^* \rangle \\ S_3 &= 2\text{Re}\langle E_H E_V^* \rangle = 2\text{Im}\langle E_L E_R^* \rangle \\ S_4 &= -2\text{Im}\langle E_H E_V^* \rangle = -\langle |E_L|^2 - |E_R|^2 \rangle. \end{aligned} \quad (6)$$

In these expressions, E is the (complex) voltage in the subscripted polarization, $*$ denotes complex conjugate, $\langle \dots \rangle$ denotes averaging (multilooking in the SAR context), and Re and Im select the real or the imaginary value (respectively) of the complex cross-product amplitude.

Several useful child parameters may be calculated from the Stokes parameters measured in the backscattered field. Four examples of these are the *degree of polarization*

$$m = (S_2^2 + S_3^2 + S_4^2)^{1/2} / S_1 \quad (7)$$

the *circular polarization ratio*

$$\mu_C = (S_1 - S_4) / (S_1 + S_4), \quad 0 \leq \mu_C \quad (8)$$

the *relative phase* between the two linear E -vectors of the backscattered field

$$\delta = \text{atan}(S_4/S_3), \quad -180^\circ < \delta \leq 180^\circ \quad (9)$$

where the $-$ or $+$ sign of the phase indicates the rotation direction of the elliptically polarized field (R and L , respectively), and the *degree of linear polarization*

$$m_L = (S_2^2 + S_3^2)^{1/2} / S_1, \quad 0 \leq m_L. \quad (10)$$

These child parameters convey information according to the characteristics of the scene, primarily its geometric shape, roughness, dielectric properties, density, or electromagnetic penetrability. Thus, the Stokes parameter values provide invaluable insight into the geophysical properties of the surface. For example, the μ_C parameter (CPR) is the traditional indicator of frozen volatile deposits [41], although it may also be anomalously large in response to backscatter from large blocky surface structures.

REFERENCES

- [1] J. N. Goswami and M. Annadurai, "Chandrayaan-1: India's first planetary science mission to the moon," *Current Sci.*, vol. 96, pp. 486–491, 2009.
- [2] G. Chin, S. Brylow, M. Foote, J. Garvin, J. Kasper, J. Keller, M. Litvak, I. Mitrofanov, D. Paige, R. K. Raney, M. Robinson, A. Sanin, D. Smith, H. Spence, P. Spudis, S. A. Stern, and M. T. Zuber, "Lunar Reconnaissance Orbiter overview: The instrument suite and mission," *Space Sci. Rev.*, vol. 129, pp. 391–419, 2007.
- [3] R. K. Raney, "Hybrid-polarity SAR architecture," in *Proc. IEEE Geosci. Remote Sens. Symp.*, Denver, CO, 2006, pp. 3846–3848.
- [4] R. K. Raney, "Hybrid-polarity SAR architecture," *IEEE Trans. Geosci. Remote Sens.*, vol. 45, no. 11, pt. 1, pp. 3397–3404, Nov. 2007.
- [5] M. E. Nord, T. L. Ainsworth, J.-S. Lee, and N. J. S. Stacy, "Comparison of compact polarimetric synthetic aperture radar modes," *IEEE Trans. Geosci. Remote Sens.*, vol. 47, no. 1, pt. 1, pp. 174–188, Jan. 2009.
- [6] R. K. Raney, "Radar fundamentals: Technical perspective," in *Principles and Applications of Imaging Radar, Manual of Remote Sensing*, F. Henderson and A. Lewis, Eds., 3rd ed. New York: Wiley Interscience, 1998, pp. 9–130.
- [7] P. E. Green, Jr., "Radar measurements of target scattering properties," in *Radar Astronomy*, J. V. Evans and T. Hagfors, Eds. New York: McGraw-Hill, 1968, pp. 1–78.
- [8] S. J. Ostro, "Planetary radar astronomy," in *The Encyclopedia of Physical Science and Technology*, vol. 12, R. A. Meyers, Ed., 3rd ed. New York: Academic, 2002, pp. 295–328.
- [9] D. B. Campbell, R. S. Hudson, and J.-L. Margot, "Advances in Planetary Radar Astronomy, Chapter 35," in *Review of Radio Science, 1999–2002*, R. Stone, Ed. Oxford, U.K.: URS, 2002, pp. 869–899.
- [10] G. G. Stokes, "On the composition and resolution of streams of polarized light from different sources," *Trans. Cambridge Philosoph. Soc.*, vol. 9, pp. 399–416, 1852.
- [11] E. Wolf, "Optics in terms of observable quantities," *Nuovo Cimento*, vol. 12, pp. 884–888, 1954.
- [12] N. J. S. Stacy and D. B. Campbell, "Stokes vector analysis of lunar radar backscatter," in *Proc. IEEE Geosci. Remote Sens. Symp.*, Tokyo, Japan, 1993, pp. 30–33.
- [13] L. M. Carter, D. B. Campbell, and B. A. Campbell, "Searching for surficial deposits on Venus using multi-polarized radar," in *Proc. Annu. Lunar Planetary Sci. Conf.*, 2003, No. 1809.
- [14] L. M. Carter, D. B. Campbell, and B. A. Campbell, "Physical properties of volcanic deposits on Venus from radar polarimetry," in *Proc. Lunar Planetary Sci. Conf.*, 2005, No. 1745.

- [15] W. T. K. Johnson, "Magellan imaging radar mission to Venus," *Proc. IEEE*, vol. 79, no. 6, pp. 777–790, Jun. 1991.
- [16] G. H. Pettengill, P. G. Ford, W. T. K. Johnson, R. K. Raney, and L. A. Soderblom, "Magellan: Radar performance and data products," *Science*, vol. 252, pp. 260–265, 1991.
- [17] R. K. Raney, A. P. Luscombe, E. J. Langham, and S. Ahmed, "RADARSAT," *Proc. IEEE*, vol. 79, no. 6, pp. 839–849, Jun. 1991.
- [18] D. L. Evans, W. Alpers, A. Cazenave, C. Elachi, T. Farr, D. Glackin, B. Holt, L. Jones, W. T. Liu, W. McCandless, Y. Menard, R. Moore, and E. Njoku, "Seasat—A 25-year legacy of success," *Remote Sens. Environ.*, vol. 94, pp. 384–404, 2005.
- [19] H. C. MacDonald, "Geological evaluation of radar imagery from Darien Province, Panama," *Modern Geol.*, vol. 1, pp. 1–62, 1969.
- [20] E. P. W. Attema, Y.-L. Desnos, and G. Duchossois, "Synthetic aperture radar in Europe: ERS, Envisat, and beyond," in *APL Tech. Dig.*, 2000, vol. 21, pp. 155–161.
- [21] P. C. Dubois and L. Norikane, "Data volume reduction for imaging radar polarimetry," in *Proc. Int. Geosci. Remote Sens. Symp.*, Ann Arbor, MI, 1987, pp. 691–696.
- [22] J. J. van Zyl and C. V. Burnette, "Data volume reduction for single-look polarimetric imaging radar data," *IEEE Trans. Geosci. Remote Sens.*, vol. 29, no. 5, pp. 784–786, May 1991.
- [23] J. J. van Zyl, H. A. Zebker, and C. Elachi, "Imaging radar polarization signatures: Theory and observation," *Radio Sci.*, vol. 22, pp. 529–543, 1987.
- [24] P. D. Spudis, C. L. Lichtenberg, B. Marinelli, and S. Nozette, "Mini-SAR: An imaging radar for the Chandrayaan-1 mission to the Moon," in *Proc. Lunar Planetary Sci. Conf.*, 2005, No. 1153.
- [25] T. H. Joo and D. N. Held, "An adaptive quantization method for burst mode synthetic aperture radar data," in *Proc. Int. Radar Conf.*, Arlington, VA, 1985, pp. 385–390.
- [26] S. N. Madsen and H. A. Zebker, "Imaging Radar Interferometry," in *Manual of Remote Sensing, 3rd Edition Principles and Applications of Imaging Radar*, vol. 2, F. M. Henderson and A. J. Lewis, Eds. New York: Wiley, 1998, pp. 359–380.
- [27] M. A. Richards, "A beginner's guide to interferometric SAR concepts and signal processing," *IEEE Aerosp. Electron. Syst. Mag.*, vol. 22, no. 9, pt. 2, pp. 5–29, Sep. 2007.
- [28] R. Hanssen, *Radar Interferometry: Data Interpretation and Error Analysis*. Dordrecht, The Netherlands: Kluwer, 2001.
- [29] J. C. Curlander and R. N. McDonough, *Synthetic Aperture Radar: Systems and Signal Processing*. New York: Wiley, 1991.
- [30] R. K. Raney, "Chapter 18, space-based remote sensing radars," in *The Radar Handbook*, M. Skolnik, Ed., 3rd ed. New York: McGraw-Hill, 2008.
- [31] R. S. Symons, "Modern microwave power modules," *IEEE Aerosp. Electron. Syst. Mag.*, vol. 17, no. 1, pp. 19–26, Jan. 2002.
- [32] T. A. Weil and M. Skolnik, "The radar transmitter, chapter 10," in *The Radar Handbook*, M. Skolnik, Ed., 3rd ed. New York: McGraw-Hill, 2008.
- [33] R. Kwok and W. T. K. Johnson, "Block adaptive quantization of Magellan SAR data," *IEEE Trans. Geosci. Remote Sens.*, vol. GRS-27, no. 4, pp. 375–383, Jul. 1989.
- [34] A. Luscombe, A. Thompson, P. James, and P. Fox, "Calibration techniques for the RADARSAT-2 SAR system," in *Proc. EUSAR*, Dresden, Germany, 2006.
- [35] B. Bussey and P. Spudis, *Clementine Atlas of the Moon*. Cambridge, U.K.: Cambridge Univ. Press, 2003, pp. 260–265.
- [36] G. J. Black, D. B. Campbell, and P. D. Nicholson, "Icy Galilean satellites: Modelling radar reflectivities as a coherent backscatter effect," *Icarus*, vol. 151, pp. 167–180, 2001.
- [37] J. V. Evans and T. Hagfors, *Radar Astronomy*. New York: McGraw-Hill, 1968.
- [38] W.-M. Boerner, H. Mott, E. Luneburg, C. Livingstone, B. Brisco, R. J. Brown, and J. S. Paterson, "Polarimetry in radar remote sensing: Basic and applied concepts," in *Principles and Applications of Imaging Radar*, vol. 2, F. M. Henderson and A. J. Lewis, Eds., 3rd ed. New York: Wiley, 1998.
- [39] A. Guissard, "Meuller and Kennaugh matrices in radar polarimetry," *IEEE Trans. Geosci. Remote Sens.*, vol. 32, no. 3, pp. 590–597, May 1994.
- [40] N. Wiener, "Generalized harmonic analysis," *Acta Mathematica*, vol. 5, pp. 118–258, 1930.
- [41] M. A. Slade, B. J. Butler, and D. O. Muhleman, "Mercury radar imaging: Evidence for polar ice," *Science*, vol. 258, pp. 635–640, 1992.

ABOUT THE AUTHORS

R. Keith Raney (Life Fellow, IEEE) received the B.Sc. degree in physics (with honors) from Harvard University, Cambridge, MA, in 1960, the M.Sc. degree in electrical engineering from Purdue University, West Lafayette, IN, in 1962, and the Ph.D. degree in computer, information, and control from the University of Michigan, Ann Arbor, in 1968.

Currently, he is with the Space Department, Applied Physics Laboratory, Johns Hopkins University, Laurel, MD. His research interests include novel architectures for Earth-observing, lunar, and planetary radars.

Dr. Raney is the recipient of numerous awards, including the 2007 IEEE Dennis J. Picard Medal for radar technologies and applications.



Paul D. Spudis received the B.S. degree from the Arizona State University, Tempe, in 1976, the Sc.M. degree from Brown University, Providence, RI, in 1977, and the Ph.D. degree from Arizona State University in 1982, all in geology.

Currently, he is a Senior Staff Scientist at the Lunar and Planetary Institute, Houston, TX. He was formerly with the Branch of Astrogeology, U.S. Geological Survey, Flagstaff, AZ, and the Applied Physics Laboratory, Johns Hopkins University, Laurel, MD. Since 1982, he has specialized in research on the processes of impact and volcanism on the planets and studies of the requirements for sustainable human presence on the Moon. He is a former member of the Committee for Planetary and Lunar Exploration (COMPLEX), an advisory committee of the National Academy of Sciences, and the Synthesis Group, a White House panel that, in 1990–1991, analyzed a return to the Moon to establish a base and the first human mission to Mars. He was Deputy Leader of the Science Team for the Department of Defense



Clementine mission to the Moon in 1994, the Principal Investigator of the mini-SAR imaging radar experiment on the Indian Chandrayaan-1 mission in 2008–2009, and a team member of the mini-RF imaging radar on NASA's Lunar Reconnaissance Orbiter mission (2009–present). He was a member of the President's Commission on the Implementation of U.S. Space Exploration Policy, whose report was issued June 2004, and in September 2004, he was presented with the NASA Distinguished Public Service Medal for his work on that body. He is the author or coauthor of over 100 scientific papers and three books, including *The Once and Future Moon*, a book for the general public in the Smithsonian Library of the Solar System series, and (with Ben Bussey) *The Clementine Atlas of the Moon* (Cambridge, U.K.: Cambridge Univ. Press, 2004).

Dr. Spudis is the recipient of the 2006 Von Karman Lectureship in Astronautics, awarded by the American Institute for Aeronautics and Astronautics.

Ben Bussey received the B.A. degree in physics from Oxford University, Oxford, U.K., in 1991 and the Ph.D. degree in planetary geology from University College London, London, U.K., in 1995.

Currently, he is an Assistant Group Supervisor of the Planetary Exploration Group, Applied Physics Laboratory, Johns Hopkins University, Laurel, MD. His research interests include the scientific and exploration potentials of the lunar poles. He is the Principal Investigator of a NASA lunar science institute team, and of the mini-RF radar instrument onboard the Lunar Reconnaissance Orbiter spacecraft. He is the lead author on several significant publications, including a book *The Clementine Atlas of the Moon* (Nature Publishing Group, a division of Macmillan, 2004), and archival articles such as "Constant illumination at the lunar south pole" (*Nature*, vol. 434, 2005).



Raney *et al.*: The Lunar Mini-RF Radars: Hybrid Polarimetric Architecture and Initial Results

Jason Crusan received the B.A. degree in physics, the B.E.E. degree in electrical engineering, computer option, and the Master of Computer Information System (MCIS) from Cleveland State University, Cleveland, OH, in 2000, 2002, and 2006, respectively.



Currently, he is with the Space Operations Mission Directorate, National Aeronautics and Space Administration (NASA) and is the Chief Technologist for Space Operations. During the mini-RF Program he served as the overall Contracting Officers Technical Representative (COTR) during the development phase and Program Executive during the Operations Phase. Before joining NASA, he worked for a number of government contracting companies supporting the NASA Glenn Research Center in Cleveland, OH. Since joining the NASA Headquarters Space Operations Mission Directorate in 2005, he has been leading a number of advanced technology development and flight projects.

J. Robert Jensen (Member, IEEE) received the B.A. degree in physical chemistry from Cornell College, Mount Vernon, IA, in 1973 and the Ph.D. degree in physical chemistry from the University of Wisconsin—Madison, Madison, in 1978.



He has been with the Applied Physics Laboratory, Johns Hopkins University, Laurel, MD, since 1978 and has been with the Space Department since 1989. His work has included radar system development and analysis as well as satellite communications and navigation. Space missions have included the mini-RF radar on NASA's Lunar Reconnaissance Orbiter and the transceiver navigation element of the New Horizons mission currently on its way to Pluto.

W. Marinelli, photograph and biography not available at the time of publication.

Priscilla McKerracher received the B.S. degree in physics (*cum laude*, Phi Beta Kappa) from the University of Illinois, Urbana-Champaign, Urbana, in 1981. Currently, she is working towards the M.S. degree in computer science at the Whiting School of Engineering, Johns Hopkins University, Laurel, MD.



Currently, she is a member of the Principal Staff at the Applied Physics Laboratory, Johns Hopkins University, where she is an experienced technical lead in software development for satellite ground systems.

Catherine Neish received the B.Sc. degree in physics and astronomy from the University of British Columbia, Vancouver, BC, Canada, in 2004, and the Ph.D. degree in planetary science from the University of Arizona, Tucson, in 2008.



Currently, she is a Postdoctoral Fellow at the Applied Physics Laboratory, Johns Hopkins University, Laurel, MD, working with data from the mini-RF instrument on the Lunar Reconnaissance Orbiter. Her research interests include radar observations of planetary objects, including the Moon, Earth, Venus, and Titan, and the origins of life, in particular the formation of prebiotic molecules on Saturn's moon Titan.

Marzban Palsetia received the B.E. degree in electrical engineering from University of Bombay, Bombay, India, in 1994 and the M.S. degree in electrical engineering from University of Florida, Gainesville, in 1996.



He was with Vexcel Corporation from 1996 to 2010 during which time he was involved with the design and development of remote sensing software products and systems for various synthetic aperture radar sensors, including the ones for the mini-RF missions. Currently, he is with Microsoft Corporation.

Ron Schulze (Senior Member, IEEE) received the B.Sc. degree in electrical engineering from Virginia Tech, Blacksburg, in 1989 and the M.Eng. degree in electrical engineering from The Ohio State University, Columbus, in 1991.



Currently, he is with the Space Department in the RF Engineering Group, Applied Physics Laboratory, Johns Hopkins University, Laurel, MD. His research interests include spacecraft radio-frequency system design, large deployable antennas, and calibration of synthetic aperture radars.

H. Brian Sequeira (Member, IEEE) received the M.S. degree in physics from Indian Institute of Technology, Bombay, India, in 1972, the M.Tech. degree from Indian Institute of Science, Bangalore, India, in 1974, and the Ph.D. degree in electrical engineering from the University of Delaware, Newark, in 1982.



Currently, he is the Principal Professional Staff at the Applied Physics Laboratory, Johns Hopkins University, Laurel, MD. His research interests include communications systems for near-Earth and deep space applications, and radar instruments for planetary exploration.

Helene Winters received the B.S. degree in computer science with a minor in mathematics from James Madison University, Harrisonburg, VA, in 1987 and the M.S. degree in systems engineering from the Whiting School of Engineering, Johns Hopkins University, Laurel, MD, in 2009, specializing in project management.



She is a member of the Principal Professional Staff at the Applied Physics Laboratory (APL), Johns Hopkins University, Laurel, MD. She joined APL in 1997 in the Space Science Applications Group and is now part of the Civilian Space Program Office. Her work at the Lab originally focused on ground systems for spacecraft and instruments. She has supported multiple DoD and civilian programs during her career. She is currently a program manager responsible for NASA's mini-RF instruments.